Ordering-Induced Fast Diffusion of Nanoscale Water Film on Graphene

Jae Hyun Park and N. R. Aluru*

Beckman Institute for Advanced Science and Technology, Department of Mechanical Science and Engineering, University of Illinois at Urbana−Champaign, Urbana, Illinois 61801

Received: August 4, 2009; Revised Manuscript Received: December 16, 2009

We show that ordering in nanoscale water film on a hydrophobic surface gives rise to fast diffusion of water. Specifically, as the surface coverage of water increases, the diffusion coefficient of water increases until a critical surface coverage and a further increase in surface coverage results in a decrease of water diffusion coefficient. For thin nanoscale films that form two layers of waters on a hydrophobic surface, the first layer of water forms a hexagonal structure, very similar to the ice Ih structure, that is independent of the surface coverage. As the surface coverage increases, the ordering of water molecules in the second layer increases and for a critical surface coverage the ordering in the second layer is maximized and the hydrogen bonding between first and second layers is minimal giving rise to fast diffusion. As the surface coverage further increases, the hydrogen bonding between the first and second layers increases and the diffusion coefficient of water is reduced. This "ordering-induced diffusion enhancement" on hydrophobic surfaces is contrary to the ordering-induced slow mobility in hydrophobic nanotubes (e.g., in a carbon nanotube).

Introduction

Rapid advances in surface nanotechnology have enabled the manufacturing of various nanoscale architectures on surfaces (e.g., nanolithography,[1] nanoprinting,[2] nanopatterned surfaces,[3] etc.). Surface nanotechnology processes typically use an extremely small amount of liquid where the molecular features of the liquid could play an important role. A detailed understanding of surface transport of molecularly thin (nanoscale) liquid films is required for precise manufacturing and control of nanoscale architectures on surfaces.

Spontaneous transport (diffusion) of nanoscale liquid films on solid substrates is typically a two-dimensional phenomena and it can be markedly different from the one-dimensional motion such as that typically observed in confined nanotubes[4] or the three-dimensional motion observed in bulk and thick liquid films. For example, surface diffusion of *n*-alkanes and long polyethylene glycol (PEG) submonolayers exhibits nonlinear dependence on the surface coverage, that is, the surface diffusion increases with increasing surface concentration, and then decreases abruptly.[5,6] Similarly, surface diffusion of submonolayer water films on a weak hydrophilic surface also showed nonlinear dependence on the surface coverage.[7]

In this paper, considering the ubiquitous nature of water in various surface nanotechnology processes, we investigate the diffusion of nanoscale water films on a hydrophobic surface by using extensive molecular dynamics (MD) simulations. We show that the diffusion of nanoscale water films on a hydrophobic surface also exhibits a nonlinear dependence on the surface coverage, but the molecular mechanisms governing the anomalous surface diffusion are quite different from those in the weak hydrophilic surface.

Methods

As a representative hydrophobic surface, we use freely suspended graphene, a single layer of graphite.[8,9] Graphene is modeled by using bonding potentials for stretching, bending, and torsion, and by the (6-12) Lennard-Jones (LJ) potential for nonbonding interactions. The total potential for a carbon atom in graphene is given by[10]

$$U(r_{ij},\theta_{ijk},\phi_{ijkl}) = k_m[1-\exp(-\gamma(r_{ij}-r_C))]^2 + \frac{1}{2}k_{\theta\theta}(\cos\theta_{ijk}-\cos\theta_{eq}) + \frac{1}{2}k_\phi(1-\cos 2\phi_{ijkl}) + 4\varepsilon_C\left[\left(\frac{\sigma_C}{r_{ij}}\right)^{12}-\left(\frac{\sigma_C}{r_{ij}}\right)^{6}\right] \quad (1)$$

where i is the atom of interest and j, k, and l are the adjacent atoms, θ_{ijk} is the bond angle between a triplet of atoms $i-j-k$ and ϕ_{ijkl} is defined as the angle between the ijk and the jkl planes, $k_m = 556.8$ kJ/mol, $\gamma = 16.45$ nm^{-1}, $r_C = 0.14114$ nm, $k_{\theta\theta} = 821.16$ kJ/mol, $\theta_{eq} = 120°$, $k_\phi = 89.1$ kJ/mol, $\sigma_C = 0.3390$ nm, and $\varepsilon_C = 0.2897$ kJ/mol. The potential considered here does not account for the surface reconstruction as the electronic structure of freely suspended graphene is typically insensitive to the H_2O adsorbates.[11] The graphene force field used in this study was developed by fitting experimental lattice parameters, elastic constants, and phonon frequencies for graphite.[10] Recent simulation of freely suspended graphene using many-body potential[12] also showed that graphene is quite stable without any surface reconstruction. The vertical variation of the atomic position in graphene is typically less than 0.1 nm (at $T = 330$ K).[13]

Simulations were performed using GROMACS 3.2.1[14] in an *NVT* ensemble. The size of graphene is 3.81 nm × 3.67 nm (*xy*-plane) and periodic boundary conditions were used along *x*- and *y*-directions. The *z*-position of graphene was set as $z = 0$ nm. A purely reflecting wall was placed at $z = 20$ nm to prevent the escape of the evaporated waters. An extra empty space of 5 nm height was included to neglect periodicity in the *z*-direction. Water molecules were modeled by using the extended simple point charge (SPC/E) model[15] and the interaction between the oxygen (OW) in water and the carbon (C) in

* To whom correspondence should be addressed. E-mail: aluru@illinois.edu. Tel: (217) 333-1180. Fax: (217)244-4333.

10.1021/jp907512z
Published on Web 01/22/2010

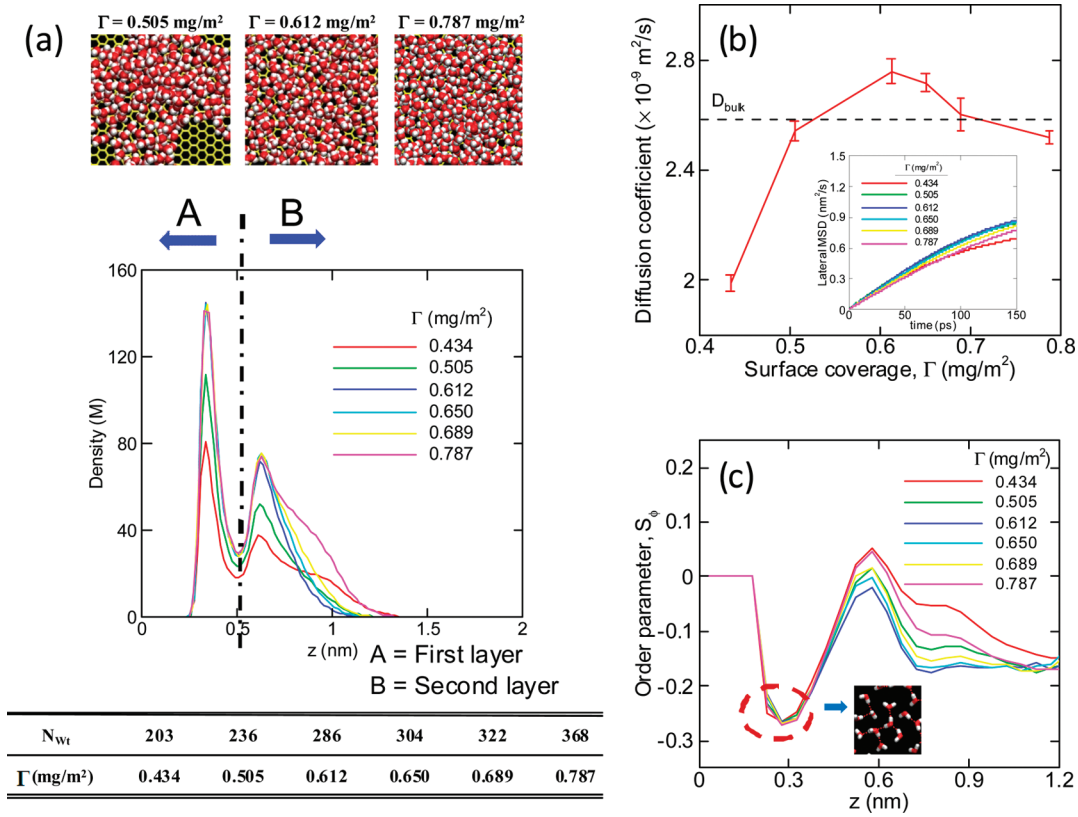

N_{Wt}	203	236	286	304	322	368
Γ (mg/m²)	0.434	0.505	0.612	0.650	0.689	0.787

Figure 1. (a) Molecular visualization of nanoscale water layers on graphene and the corresponding density plots for various surface coverages. The snapshots were rendered using VMD.[29] Γ is the surface coverage and it is defined as the ratio of the total mass of the water molecules to the surface area of graphene. The table summarizes the surface coverage conditions considered in this study. The area of the graphene sheet in MD simulation is 13.98 nm^2. N_{Wt} is the number of water molecules in the system. (b) Diffusion coefficient of water on graphene for various surface coverages and MSD plots (inset). (c) Order parameters for various surface coverages. In the snapshot (top view), the red site represents the oxygen atom while the white site represents the hydrogen atom. The red line shows the hydrogen bond between waters.

graphene was modeled using the LJ potential and $\sigma_{OW\text{-}C}$ and $\varepsilon_{OW\text{-}C}$ were computed using the Lorentz−Berthelot mixing rule: $\sigma_{OW\text{-}C} = (\sigma_{OW} + \sigma_C)/2$ and $\varepsilon_{OW\text{-}C} = (\varepsilon_{OW}\varepsilon_C)^{1/2}$. Electrostatic interactions were computed using the Particle Mesh Ewald (PME) method[16] with a two-dimensional correction.[17] All the simulations were equilibrated for 6 ns. The sampling period was 18 ns. The Nosé−Hoover thermostat[18,19] was used to maintain the system temperature at 300 K. The equation of motion was integrated by using the leapfrog algorithm with a time step of 1.0 fs.

Results and Discussion

As summarized in Figure 1a, six surface coverages (surface coverage is denoted by Γ) were considered ranging from Γ = 0.434 mg/m^2 to Γ = 0.787 mg/m^2. The surface coverage was defined as the total mass of waters per unit area of surface. In contrast to the formation of a stable water submonolayer on a hydrophilic surface,[7] a stable water monolayer cannot form on the hydrophobic surface considered in this study. Even for the smallest Γ = 0.434 mg/m^2, a double-layered structure with two density peaks was observed (see Figure 1a). This is because the solid−water interaction is not strong enough to spread out all the water molecules by fully overcoming the water−water interaction. When the amount of waters is sufficiently smaller than the maximum capacity of a single-layer on the surface, the water−water interaction has the strong tendency to gather all the water molecules together. For example, in the present study when the surface coverage is smaller than Γ = 0.434 mg/m^2 a droplet, that is, "an isolated water cluster", is formed instead of an infinitely connected water network. This is similar to the previous finding that a water monolayer is not stable under confinement between two hydrophobic objects.[20] The double-layered structure in Figure 1a can be divided into the first (region A in Figure 1a; $z < 0.5$ nm) and the second (region B in Figure 1a; $z > 0.5$ nm) layers according to the density peaks. As Γ increases, both first and second peaks grow simultaneously until their equilibrium packing densities, which occurs at Γ = 0.612 mg/m^2. The equilibrium packing density presents the water capacity of each layer. The macroscopic voids were clearly observed for Γ = 0.434 and 0.505 mg/m^2, and their size decreases with increase in Γ. The macroscopic voids were not observed for Γ > 0.612 mg/m^2. At Γ = 0.689 mg/m^2, the number of waters exceeds the capacity of the double-layered structure and the growth of an extended tail from the second density peak or the initiation of the third peak is observed. Finally, at Γ = 0.787 mg/m^2, the third peak starts to become more prominent.

The spontaneous transport of water film can be quantified by the diffusion coefficient. Figure 1b shows the lateral diffusion coefficient of water as a function of surface coverage. Lateral diffusion coefficient was obtained from the slope of the lateral mean-squared displacement (MSD) of water versus time: $D = \lim_{t\to\infty} \langle |\mathbf{R}_{CM}(t) - \mathbf{R}_{CM}(t=0)|^2 \rangle / 4t$, where $\mathbf{R}_{CM}$ is the (x, y)-position of the center-of-mass of the water molecule. Throughout this manuscript, "diffusion" coefficient refers to the "lateral diffusion" coefficient unless specified, otherwise. From Figure 1b, we observe a nonlinear Λ-behavior of diffusion coefficient. The inset shows the MSDs for various surface coverages. The MSD plots were computed by dividing the entire trajectory (after equilibrium is reached) of a molecule into several chunks and

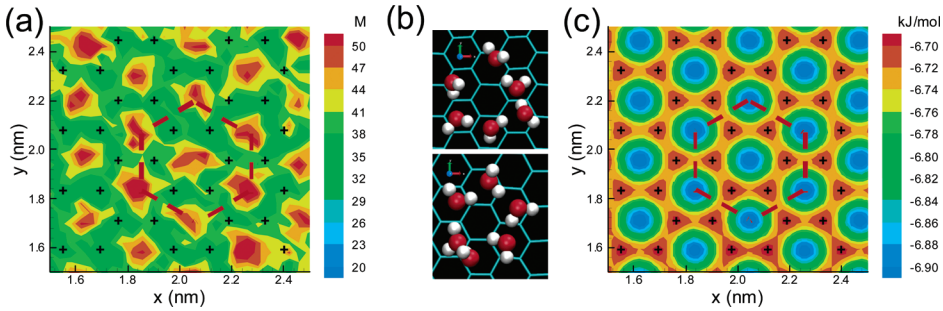

Figure 2. (a) Oxygen density map at the first density peak for $\Gamma = 0.689$ mg/m^2. (b) Representative hexagonal water rings in the first layer near the surface. The red balls represent the oxygen atom and the white balls represent the hydrogen. (c) Energy map for water-surface interaction in the first peak plane at $z = 0.33$ nm.

averaged over all the chunks. When computing diffusion coefficient, the initial transient stage was not considered and only the linear region was fitted with linear regression. Specifically, the diffusion coefficient gradually increases with the increase in surface coverage until a critical surface coverage ($\Gamma_{crit} = 0.612$ mg/m^2), beyond which the diffusion coefficient decreases with a further increase in the surface coverage. The maximum diffusion coefficient at $\Gamma = \Gamma_{crit}$ was found to be 2.76 ($\pm$0.044) $\times$ 10^{-9} m^2/s. This is about 7.3% higher than the bulk diffusion coefficient of water (2.57 ($\pm$0.009) $\times$ 10^{-9} m^2/s). The nonlinear Λ-behavior of diffusion coefficient has also been observed for the surface transport of *n*-alkanes on graphite[6] and submonolayer water films on a weak hydrophilic surface.[7] Although the trend in diffusion is similar, the liquid type and its molecular structure on the surface are different in each case and subsequently the molecular mechanism governing the nonlinear behavior is different. Considering that the water molecules on a weak hydrophilic surface form a stable submonolayer film[7] while the water molecules can form only a double layer structure on a hydrophobic surface, the molecular mechanisms governing diffusion on a hydrophilic surface can be vastly different from those on a hydrophobic surface. In the rest of this paper, we will investigate the molecular mechanisms governing the nonlinear behavior in diffusion on a hydrophobic surface. Given that the spontaneous liquid transport (diffusion) on a solid substrate is typically the result of the interplay between water−substrate and water−water interactions,[6,7] we first consider the possibility that the diffusion is dominated by water−substrate interaction. If this is the case, the water−substrate interaction should exhibit a similar trend to that of the diffusion. However, the trend in water−graphene interaction energy was found to be exactly opposite to that of diffusion, that is, lowest energy of −3.0171 kJ/mol was observed at $\Gamma_{crit} = 0.612$ mg/m^2, which implies the lowest diffusion coefficient.[21] It is thus natural to presume that the nonlinear behavior in diffusion of water films on a hydrophobic surface is primarily governed by the water−water interaction.

As a first step to understand the role of water−water interactions on the nonlinear behavior of diffusion in Figure 1b, we investigated the structural ordering in various water films by computing the order parameter in Figure 1c. The order parameter, S_ϕ, is defined as[22]

$$S_\phi = \frac{1}{2}\langle 3\cos^2\phi - 1\rangle \qquad (2)$$

where ϕ is the angle between the surface normal and the dipole vector of water (bisector of the HW−OW−HW angle). If all the water molecules are aligned parallel to the surface, $S_\phi = -0.5$. If the medium is fully random, $S_\phi = 0$. If all the water molecules are aligned normal to the surface, $S_\phi = 1.0$. In Figure 1c, the order parameter has the minimum value of $S_\phi = -0.27$ in the first layer (region A in Figure 1a; $z < 0.5$ nm), regardless of the surface coverage. The position of the minimum value ($z = 0.275$ nm) is slightly shifted toward the surface from the first density peak ($z = 0.33$ nm). The snapshot (a top view) in Figure 1c shows that the water molecules in the first layer are aligned along the *xy*-plane. In the second layer (region B in Figure 1a; $z > 0.5$ nm), the strongest ordering is observed for $\Gamma = \Gamma_{crit}$, that is, S_ϕ for Γ_{crit} is always smaller than S_ϕ for other surface coverages.

The ordering of water molecules in the first layer can be further probed by investigating the two-dimensional density map. Figure 2a depicts the density map of oxygen atom of water (OW) in the first layer for $\Gamma = 0.689$ mg/m^2. Data is sampled in the region within 0.2 nm around the first peak. In the plot, the blue color represents lower density whereas the red color represents higher density spots. The symbol denotes the position of carbon atom in graphene. The high density sites form a quite regular hexagonal mesh (see the dashed line in Figure 2a); we refer to this as two-dimensional ordering. Although the connection between high density sites looks triangular (this is because the density map was computed from the average over thousands snapshots), at each snapshot the waters in the first layer prefer to form hexagonal rings as shown in Figure 2b. This hexagonal structure in the first layer is quite similar to the structure of ice Ih.[23] Interestingly, such regularity is maintained regardless of the variation of surface coverage and it is due to the considerable water−surface interaction. Figure 2c shows the interaction energy map, which was computed by placing a water molecule at various positions in the first peak plane ($z = 0.33$ nm) and computing its interaction energy with all the carbon atoms in graphene. In the figure, the blue color represents the lower energy region (strong binding site for water) whereas the red color represents the higher energy region. The symbol denotes the position of carbon atom in graphene and it is found that the low energy position is located exactly at the center of hexagonal carbon ring. The various low energy positions form a quite regular hexagonal mesh (see the dashed line in Figure 2c). It should be noted that the high density sites (red spots in Figure 2a) coincide with the low energy positions in Figure 2c (blue spot) which is closely related with the atomic configuration of graphene. In summary, from the order parameter distribution and the density map, we observe that the water molecules in the first layer are ordered into a two-dimensional hexagonal ring regardless of the surface coverage and the water molecules in the second layer are most ordered for $\Gamma = \Gamma_{crit}$. It is quite interesting to note that the diffusion coefficient is reduced in

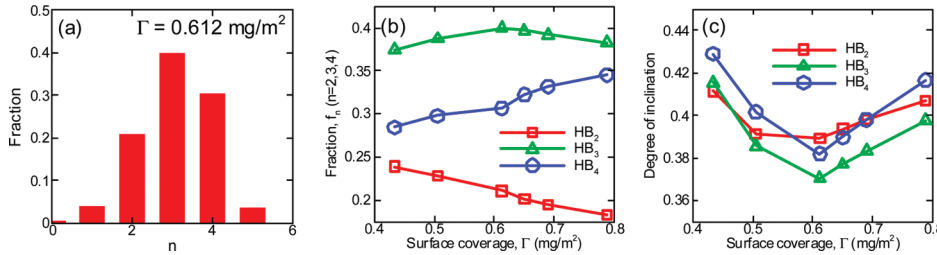

Figure 3. (a) Distribution of n-water hydrogen bonds for $\Gamma = \Gamma_{crit} = 0.612$ mg/m^2. (b) Comparison of major HB$_n$ ($n = 2, 3, 4$) for various surface coverages; (c) Degree of inclination for various surface coverages.

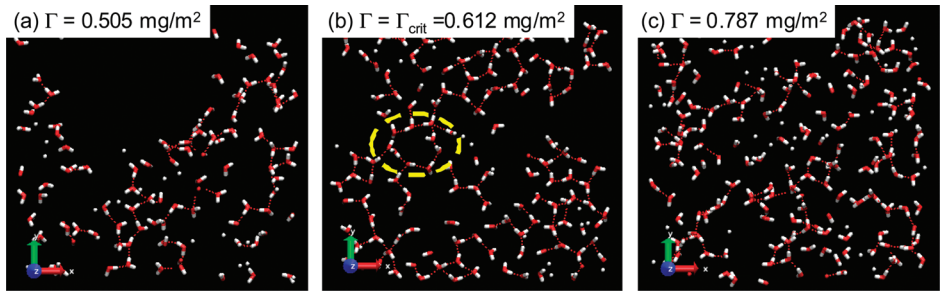

Figure 4. Top view of water structure in the second density peak region. Red lines show the HBs between waters. (a) $\Gamma = 0.505$ mg/m^2; (b) $\Gamma = \Gamma_{crit} = 0.612$ mg/m^2; (c) $\Gamma = 0.787$ mg/m^2.

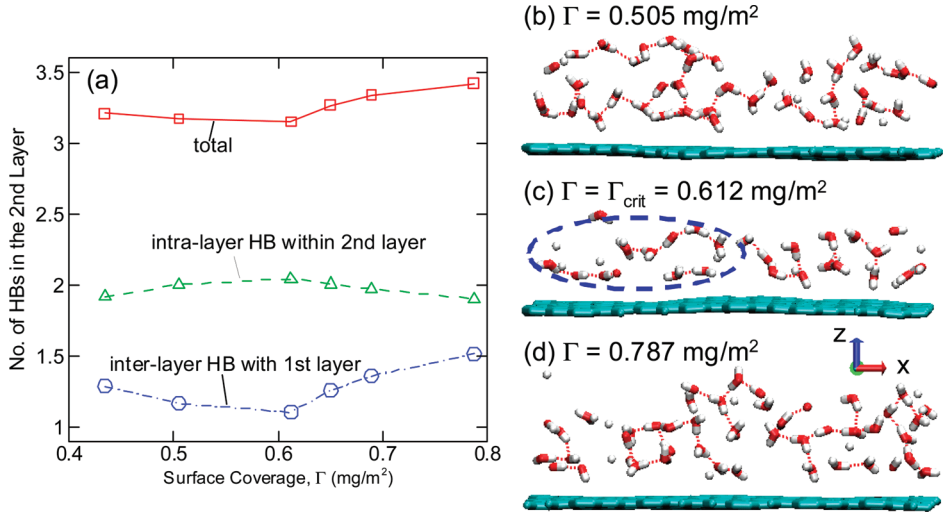

Figure 5. (a) Contributions from intralayer HB and interlayer HB with the first layer on the HBs in the second layer. (b) Molecular visualization of hydrogen bonding between first and second layers of water for $\Gamma = 0.505$ mg/m^2. Red lines show the HBs between waters. (c) $\Gamma = \Gamma_{crit} = 0.612$ mg/m^2. (d) $\Gamma = 0.787$ mg/m^2.

the three-dimensionally ordered water network (e.g., ice) while for the present two-dimensionally ordered water network, it is enhanced! Next, we will explain why the diffusion becomes maximum for the most ordered state by considering the hydrogen bonding properties of water.

The water−water hydrogen bond (HB) can be defined by using a geometrical criterion.[24] For a pair of water molecules, the hydrogen atom forms the hydrogen bond if the following two conditions are simultaneously fulfilled: (1) the distance between oxygen atoms is less than 3.5 Å, and (2) the angle between the OW−OW vector and the OW−HW vector does not exceed 30°. Figure 3a shows the distribution of n-water hydrogen bonds (if a water molecule is involved in n hydrogen bonds (e.g., $n = 2$, 3, etc.), it is referred to as n-water hydrogen bonding) for $\Gamma = \Gamma_{crit} = 0.612$ mg/m^2. We observe that there are three major HB modes with two, three, and four water molecules. For all the surface coverage cases, these three HB modes are dominant over the other modes. Hereafter, for simplicity, we denote HB$_n$ as the HB with n-water HBs (e.g., HB$_2$, HB$_3$, and HB$_4$, etc.). Figure 3b compares f_n with $n = 2$, 3, 4 for various surface coverages. f_n is the fraction of HB$_n$. Among the three major HB modes, the behavior of HB$_3$ is found to be quite similar to that of diffusion (maximum at $\Gamma = \Gamma_{crit}$). In other words, HB$_3$ can be interpreted as the "diffusion-determining HB mode". Considering the tetrahedral nature of HB network in bulk water,[25] HB$_4$ can be regarded as a representation of three-dimensional features of HB network in water films. f_4 increases with Γ implying that the three-dimensional contribution increases with increase in Γ. However, f_2 decreases with increase in Γ. In contrast to bulk water where HB$_2$ is negligible,[26] a considerable amount of HB$_2$ was observed and this is due to the water molecules on the boundaries of macroscopic void as well as on gas−water interface. The decrease in f_2 implies the reduction in contribution of the macroscopic void and gas−water interface. It should be noted that the fraction of HB$_2$ is small when compared to that of HB$_3$ and HB$_4$.

The geometrical features of each HB mode can be quantified by computing the degree of inclination. The oxygen−oxygen distance between two hydrogen-bonded water molecules is decomposed into its in-plane and out-of-plane components. For two oxygens identified by OW_i (x_i, y_i, z_i) and OW_j (x_j, y_j, z_j), the in-plane distance is computed as $r_{||} = [(x_i - x_j)^2 + (y_i - y_j)^2]^{1/2}$ while the out-of-plane distance is computed as $r_{\perp} = |z_i - z_j|$ (recall that the hydrophobic surface lies in the xy-plane). Then, we define the degree of inclination as the ratio of $r_{\perp}$ to $r_{||}$, which indicates how the HB is inclined against the xy-plane. Figure 3c compares the degree of inclination for various surface coverages. Of the three major HB modes, HB_3 has the smallest degree of inclination, that is, HB_3 is most aligned along the surface. Also, the degree of inclination for HB_3 is minimum at $\Gamma = \Gamma_{crit}$.

The top view of the water structure in the second density peak region is illustrated in Figure 4 for three surface coverages, $\Gamma = 0.505$ mg/m^2, $\Gamma = \Gamma_{crit} = 0.612$ mg/m^2, and $\Gamma = 0.787$ mg/m^2. We observe that the majority of HB_3 in the Γ_{crit} case are such that they form a planar structure of water rings (see the yellow dashed circle), which is similar to the regular hexagonal structure in the first density peak (see Figure 2a).

The HBs also influence the interplay between the first and the second layers. Figure 5a shows the number of HBs in the second layer ($z > 0.5$ nm) and the contribution from intralayer HB (within the second layer) and from interlayer HB (with the first layer). The interplay between the first and second layers is minimum at $\Gamma = \Gamma_{crit}$ due to the planar geometrical configuration as discussed in Figure 3. This can also be confirmed by examining the molecular visualizations as shown in Figure 5b−d for three surface coverages of $\Gamma = 0.505$ mg/m^2, $\Gamma = \Gamma_{crit} = 0.612$ mg/m^2, and $\Gamma = 0.787$ mg/m^2. As observed in the figures, for $\Gamma = \Gamma_{crit}$ many intralayer HBs were observed (see the blue dashed circle) while for the other two cases, the interlayer HBs between the first and the second layers is significant. As a result, the diffusion coefficient of water is maximum for the $\Gamma = \Gamma_{crit}$ case.

Conclusion

In summary, the diffusion of nanoscale water films on a hydrophobic surface (graphene) shows a nonlinear Λ-behavior depending on the surface coverage. At the critical surface coverage, where the diffusion is maximum, the water structure is most-ordered. Of the three major HB modes, the contribution of HB_3 with planar geometry is significant compared to HB_2 and HB_4, that is, larger diffusion coefficient originates from the higher fraction of HB_3. In addition, the second layer has more effect on the diffusion than the first layer in which the water-surface interaction is considerable. Water behavior in closed confinement (1D diffusion) has been extensively studied.[27,28] However, surface diffusion (2D diffusion) of water on hydrophobic surfaces has not received much attention. The diffusion of water inside hydrophobic carbon nanotube (CNT) becomes critically slow when the structure is ordered.[4] In contrast, in the present study on surface diffusion of water on a hydrophobic surface, we observed "ordering-induced" fast diffusion of water. This fundamental finding can help in design of various nanoscale processes on hydrophobic surface.

Acknowledgment. This research was supported by NSF under Grants 0120978, 0328162, 0810294, 0852657, and 0915718 and by NIH under Grant PHS 2 PN2 EY016570B.

References and Notes

(1) Salaita, K.; Wang, Y.; Mirkin, C. A. *Nat. Nanotechnol.* **1990**, *2*, 145–155.
(2) Kraus, T.; Malaquin, L.; Schmid, H.; Riess, W.; Spencer, N. D.; Wolf, H. *Nat. Nanotechnol.* **2007**, *2*, 570–576.
(3) Wang, J. Z.; Zheng, Z. H.; Li, H. W.; Huck, W. T. S.; Sirringhaus, H. *Nat. Mater.* **2004**, *3*, 171–176.
(4) Mashl, R. J.; Joseph, S.; Aluru, N. R.; Jakobsson, E. *Nano Lett.* **2003**, *3*, 589–592.
(5) Zhao, J.; Granick, S. *J. Am. Chem. Soc.* **2004**, *126*, 6242–6243.
(6) Park, J. H.; Aluru, N. R. *Chem. Phys. Lett.* **2007**, *447*, 310–315.
(7) Park, J. H.; Aluru, N. R. *Appl. Phys. Lett.* **2008**, *93*, 253104.
(8) Novoselov, K. S.; Geim, A. K.; Morozov, S. V.; Jiang, D.; Zhang, Y.; Dubonos, S. V.; Grigorieva, I. V.; Firsov, A. A. *Science* **2004**, *306*, 666–669.
(9) Novoselov, K. S.; Jiang, D.; Schedin, F.; Booth, T. J.; Khotkevich, V. V.; Morozov, S. V.; Geim, A. K. *Proc. Natl Acad. Sci. U.S.A.* **2005**, *102*, 10451–10453.
(10) Guo, Y.; Karasawa, N.; Goddard, W. A., III. *Nature* **1991**, *351*, 464–467.
(11) Wehling, T. O.; Lichtenstein, A. I.; Katsnelson, M. I. *Appl. Phys. Lett.* **2008**, *93*, 202110.
(12) Fasolino, A.; Los, J. H.; Katsnelson, M. I. *Nat. Mater.* **2007**, *6*, 858–861.
(13) Liu, P.; Zhang, Y. W. *Appl. Phys. Lett.* **2009**, *94*, 231912.
(14) Lindahl, E.; Hess, B.; van der Spoel, D. *J. Mol. Model.* **2001**, *7*, 306–317.
(15) Berendsen, H. J. C.; Grigera, J. R.; Staatsma, T. P. *J. Phys. Chem.* **1987**, *91*, 6269–6271.
(16) Darden, T.; York, D.; Pedersen, L. *J. Chem. Phys.* **1993**, *98*, 10089–10092.
(17) Yeh, I.-C.; Berkowitz, M. L. *J. Chem. Phys.* **1999**, *111*, 3155–3162.
(18) Nosé, S. *Mol. Phys.* **1984**, *52*, 255–268.
(19) Hoover, W. G. *Phys. Rev. A* **1985**, *31*, 1695–1697.
(20) Wallqvist, A.; Berne, B. J. *J. Phys. Chem.* **1995**, *99*, 2893–2899.
(21) Soon, A.; Wong, L.; Lee, M.; Todorova, M.; Delly, B.; Stampfl, C. *Surf. Sci.* **2007**, *601*, 4775–4785.
(22) Stöckelmann, E.; Hentschke, R. *J. Chem. Phys.* **1999**, *110*, 12097–12107.
(23) Fletcher, N. H. *The Chemical Physics of Ice*; Cambridge University Press: London, UK, 1970.
(24) Luzar, A.; Chandler, D. *Nature* **1996**, *379*, 55–57.
(25) Bernal, J. D.; Fowler, R. H. *J. Chem. Phys.* **1933**, *1*, 515–6271.
(26) Chandra, A.; Chowdhuri, S. *Proc. Indian Acad. Sci. (Chem. Sci.)* **2001**, *113*, 591–601.
(27) Rasaiah, J. C.; Garde, S.; Hummer, G. *Annu. Rev. Phys. Chem.* **2008**, *59*, 713–740.
(28) Joseph, S.; Aluru, N. R. *Nano Lett.* **2008**, *8*, 452–458.
(29) Humphrey, W.; Dalke, A.; Schulten, K. *J. Mol. Graphics* **1996**, *14*, 33–38.

JP907512Z